Ultrasonics Sonochemistry 75 (2021) 105611

Contents lists available at ScienceDirect

Ultrasonics Sonochemistry

journal homepage: www.elsevier.com/locate/ultson

Acoustic resonance and atomization for gas-liquid systems in microreactors

Keiran Mc Carogher [a], Zhengya Dong [a,1,2], Dwayne S. Stephens [b,2], M. Enis Leblebici [c], Robert Mettin [b], Simon Kuhn [a,*]

[a] KU Leuven, Department of Chemical Engineering, Celestijnenlaan 200F, 3001 Leuven, Belgium
[b] Drittes Physikalisches Institut, Georg-August-Universität Göttingen, Friedrich-Hund-Platz 1, 37077 Göttingen, Germany
[c] Center for Industrial Process Technology, Department of Chemical Engineering, KU Leuven, Agoralaan Building B, 3590 Diepenbeek, Belgium

ARTICLE INFO

Keywords:
Acoustic resonance
Microreactors
Gas-liquid Taylor flow
Atomization
Gas-liquid mass transfer

ABSTRACT

It is shown that a liquid slug in gas–liquid segmented flow in microchannels can act as an acoustic resonator to disperse large amounts of small liquid droplets, commonly referred to as atomization, into the gas phase. We investigate the principles of acoustic resonance within a liquid slug through experimental analysis and numerical simulation. A mechanism of atomization in the confined channels and a hypothesis based on high-speed image analysis that links acoustic resonance within a liquid slug with the observed atomization is proposed. The observed phenomenon provides a novel source of confined micro sprays and could be an avenue, amongst others, to overcome mass transfer limitations for gas–liquid processes in flow.

1. Introduction

Despite the potential microreactors have shown with regards to industrially relevant applications that are mass transfer limited, highly exothermic and/or dangerous [1–6], practical implementation has been somewhat limited. As traditional scaling techniques [7,8] are either not feasible or require precise and complex designs to assure uniform phase distribution, alternative strategies such as process intensification are sought after to increase productivity at smaller scales [9]. When ultrasound and microfluidics are combined correctly, the benefits are apparent as their cumulative performance is often better than the sum of the technologies applied separately [10–13]. Productivity is increased and, for systems with solids present, operation times can be extended considerably as microchannel clogging and fouling are mitigated through the effects of ultrasound [14,15]. Thirdly, these effects can be utilized to develop new processing techniques [16–20] that would supply the demand for novel continuous reaction systems in the fine chemical industry.

For continuous gas–liquid systems in microreactors, ultrasound has already demonstrated an improvement in processing capability [21–24]. More specifically, the varying pressure fields driven by ultrasonic oscillations can excite cavitation [25,26] and/or surface waves on the introduced gas bubbles, increasing the specific surface area available for mass transfer [27]. Secondly, this type of bubble oscillation behaviour induces pressure and velocity fluctuations in the surrounding liquid resulting in steady streaming flow, referred to as cavitation microstreaming [28]. Both these effects have helped lessen the adverse attributes typically associated with gas–liquid processing in microreactors, viz. poor convective mixing and low gas solubility. In this paper we go beyond these two effects, demonstrating a method that increases interfacial area to much larger extents at practical ultrasonic power inputs, avoiding the need for excessive cooling and energy consumption. This increase is realised through significant amounts of atomization that occurs when the liquid slugs are in a state of acoustic resonance. Previously [15,29] ultrasonic resonance in microfluidic devices has been established at frequencies ranging from 1 MHz and higher where the acoustic wavelength matches that of the channel width and/or depth. At these high frequencies, the effects of cavitation in microchannels are limited [15]. Here we demonstrate through experimental and numerical analysis that resonance can be established within a liquid slug in gas–liquid segmented (Taylor) flow, see Fig. 1. This is achieved at lower ultrasonic frequencies where cavitation effects prevail, possibly causing the observed atomization phenomena. These novel observations would offer new insights on the mechanisms of atomization as well as improving the efficiency of ultrasound in microreactors.

* Corresponding author.
E-mail address: simon.kuhn@kuleuven.be (S. Kuhn).
[1] Current Address: Chemistry and Chemical Engineering Guangdong Laboratory, Haibin Road 12, Jinping District, 515063 Shantou, China.
[2] These authors contributed equally.

https://doi.org/10.1016/j.ultsonch.2021.105611
Received 20 March 2021; Accepted 27 May 2021
Available online 1 June 2021

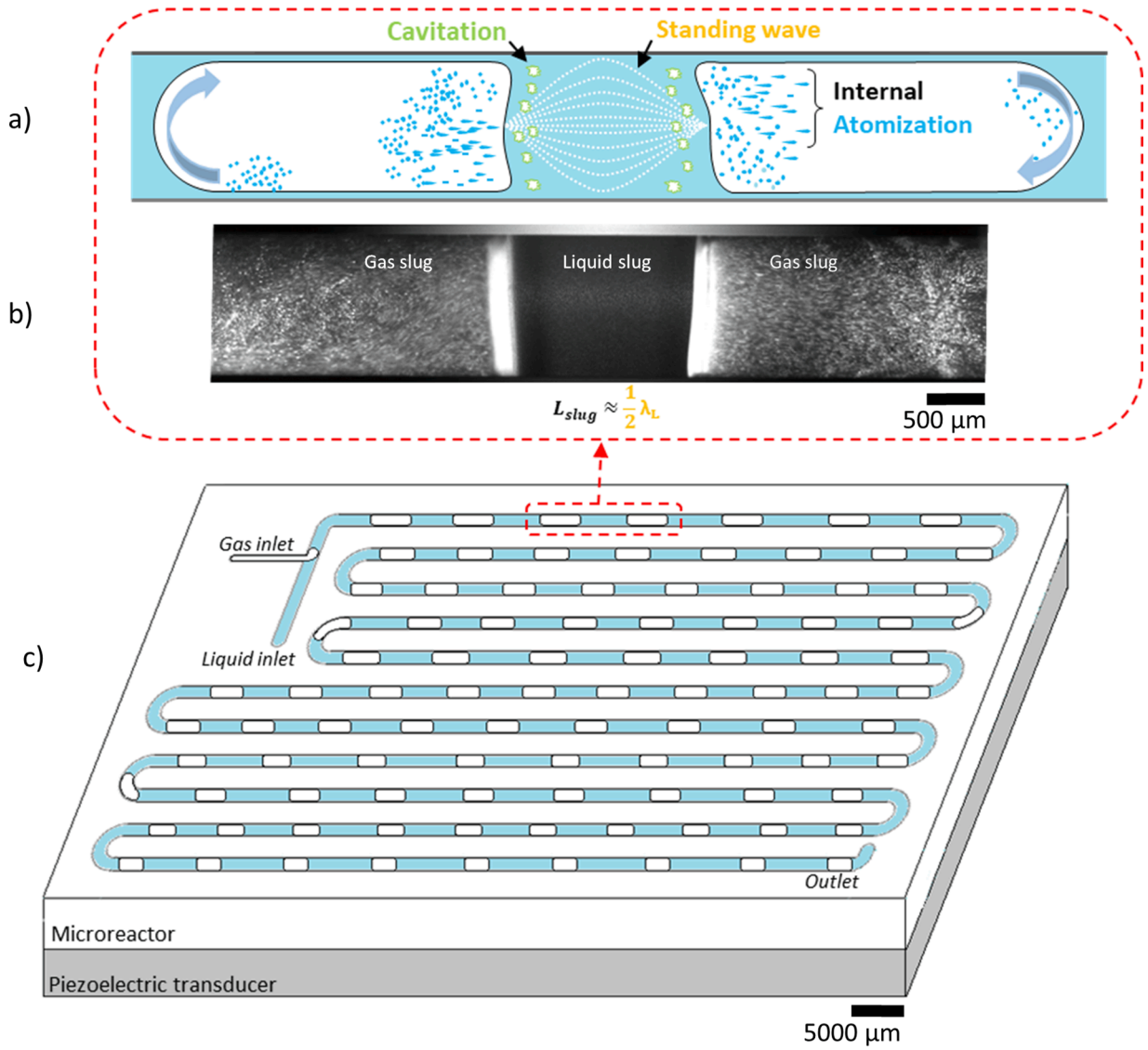

Fig. 1. a) Schematic representation of resonance and atomization within liquid and gas slugs in segmented flow. b) Image of a resonating liquid slug and atomization occurring in the gas slug. c) Depiction of gas–liquid segmented flow in the ultrasonic microreactor used to conduct the experiments in this work.

2. Materials and methods

2.1. Experimental setup

Three reactors were used during this study. The first comprised of a silicone etched microreactor bonded to a piezoelectric transducer which allowed for a high acoustic transmission to the reactor channels [30] as well as a well-defined structure for the acoustic simulations. The second and third reactors comprised of a glass capillary bonded to a piezoelectric transducer of a distinct geometry to assure distinct resonance/operating frequencies. Although acoustic transmission was lower for the glass capillary reactors the channels were visibly more accessible, allowing for better illumination to study the mechanisms of atomization.

For the silicone etched reactor a meandering square channel was etched into the silicone plate (77 × 40 × 1.74 mm^3, LTF GmbH, Germany) via deep ion etching with a width, depth and total length of 1.2 mm, 0.6 mm and 740 mm respectively connected by circular bends of 1.67 mm centre radius. A glass plate cover (77 × 40 × 1.16 mm^3) was anodically bonded to the top of the silicone plate to seal the channel and a piezoelectric transducer (Pz26, 80 × 40 × 4.06 mm^3, Ferroperm, Denmark) glued to the bottom. A detailed sketch of the microreactor with its dimensions can be found in Fig. S1. a) in the ESI. For the two glass capillary reactors a single glass capillary (VitroTubes, 1 mm square ID, 1.2 mm square OD, 100 mm) was glued (301 epoxy, Epotek) to a piezoelectric transducer (Pz26, 20 × 11 × 1.67 mm^3 and 80 × 20 × 1.67 mm^3, Ferroperm, Denmark), the sketch with dimensions can be found in Fig S1. c) and d) in the ESI.

Using an impedance analyser (16777 k, SinePhase) the resonance, and therefore, operating frequencies of the reactors were obtained. The impedance curve of the silicone etched reactor, depicted in Fig. S2 in the ESI, indicated three significant resonance peaks at 47, 411 and 601 kHz. For the glass capillary reactors significant resonance peaks were observed at 86, 156.5 and 439 kHz. Ultrasound was actuated by connecting the reactors to a power amplifier (RF 2100L, 100 W, E&I) and signal generator (33500B, Keysight) which generated a sinusoidal waveform with a selected amplitude at the reactor's resonant frequencies. The oscillation amplitude was then selected to achieve the desired load power to the reactors. Gas-liquid Taylor flow was obtained by feeding carbon dioxide (>99.5 vol%, Air Liquide) and deionized water into an internal T-junction for the silicone etched reactor and an external T-junction for the glass capillary reactors. The flow rate of carbon dioxide coming from the gas cylinder was controlled by a mass flow controller (EL-FLOW, Bronkhorst), while the flow rate of deionized water was controlled by a syringe pump (Fusion 200, KR Analytical),

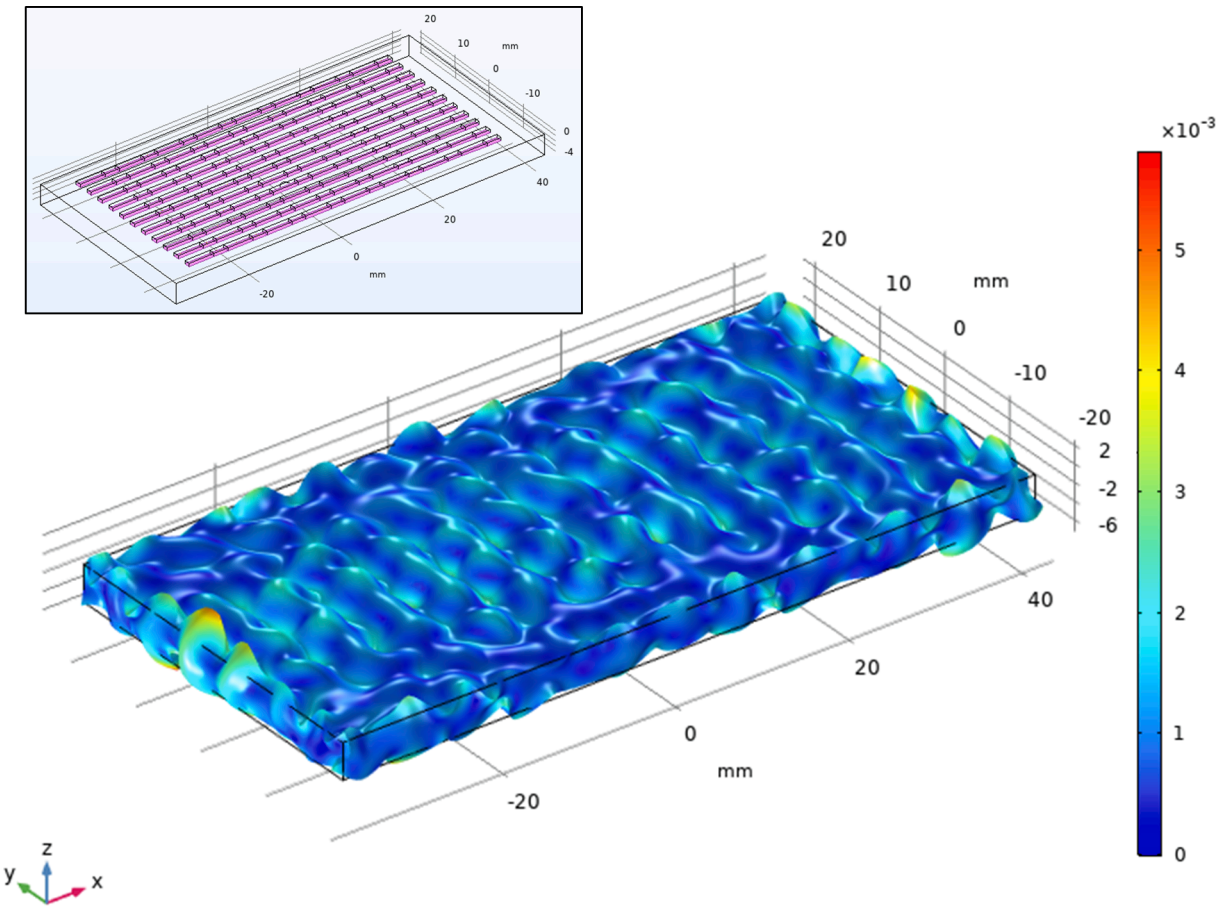

Fig. 2. Surface displacement of the piezoelectric transducer at 411.8 kHz with 1 V electric potential applied, the unit scale of the colour-bar is in μm. Top left overlay: Channels comprised of liquid and gas segments on top of the piezo. The pink surfaces represent the identity pair between the piezo and the bottom of the channels. An enlarged image of the liquid and gas segments and the identity pair can be found in the ESI, see Fig. S4. (For interpretation of the references to colour in this figure legend, the reader is referred to the web version of this article.)

with PFA tubing (OD 1/16″, ID 1 mm) serving as the flow lines to and from the reactor.

The effects of ultrasound on the gas–liquid Taylor flow pattern were observed by placing the reactors beneath a high-speed camera (Photron Mini, UX100), which was attached to either a macro zoom lens (Macro AF90 Tamron) for an overview of the reactor or a micro zoom lens (P2-SHR Plan Apo 1x, Nikon) for a more detailed view inside the micro-channels. For the silicone etched reactor the light source was placed above the reactor and for the glass capillary reactors the light source was placed below the capillary as it protruded from the transducer, allowing for better illumination and higher frame rates. The schematic of the experimental setup can be found in Fig. S1. e) in the ESI. Images were then processed using ImageJ.

2.2. Numerical methods

The sound field inside the channels of the silicone etched reactor was simulated using the finite element software COMSOL Multiphysics V5.5 (Comsol AB, Stockholm, Sweden). In order to achieve this, the problem was divided into two parts. First, the displacement of the piezoelectric transducer plate under a driving voltage U and frequency f was modelled. Second, the displacement results from the first step were used as a boundary condition to determine the sound field inside the channels at the same frequency.

2.3. Displacement simulations

The solid mechanics, electrostatics module and their predefined multiphysics coupling, "piezo electric effect", were used. The piezoelectric transducers material properties, summarised in the ESI section S2, were obtained from Anderson *et al.* [31]. The constitutive piezoelectric equations in their stress-charge form are

$$T = c_E S - eE \tag{1}$$

$$D = eS + \varepsilon_S E \tag{2}$$

where T is the stress (N/m^2), S is the strain, E is the electric field (V/m), D is the electric displacement (C/m^2), c_E is the elasticity matrix (N/m^2), e is the coupling matrix (C/m^2) and ε_S is the permittivity matrix (F/m).

A Rayleigh damping formulation was used with

$$\alpha = 0 \tag{3}$$

$$\beta = \frac{1}{\omega Q_m} \tag{4}$$

where Q_m is the mechanical quality factor and $\omega = 2\pi f$. This was included by adding a "Rayleigh damping" node under "Piezoelectric material 1" in COMSOL [31]. The factors α and β essentially correspond to low and high frequency damping, respectively. Here, only high frequencies are relevant. A numerical impedance analysis of the piezoceramic plate indicated resonance peaks at 49.2 and 411.8 kHz, which corresponded well with the experimentally measured resonance frequencies of the piezoelectric transducer used for this reactor.

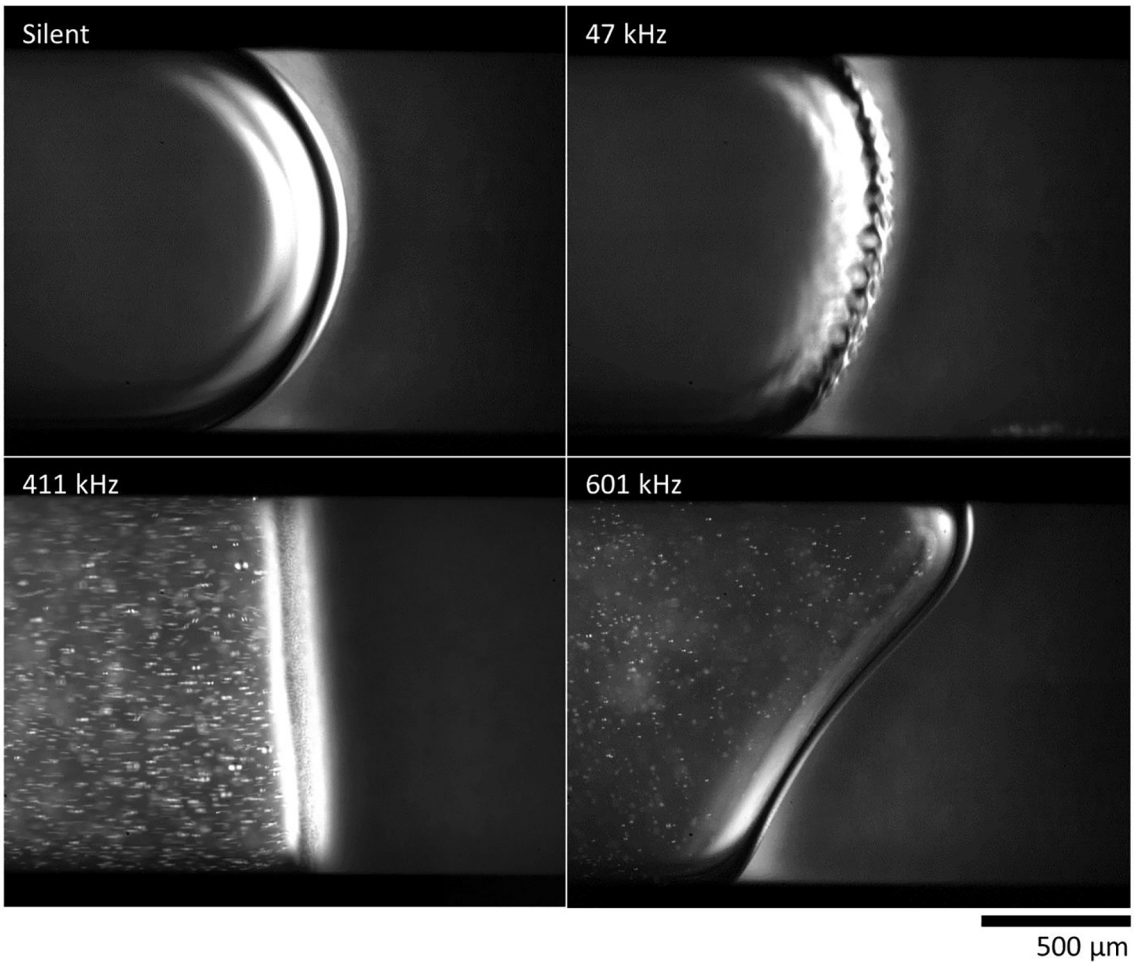

Fig. 3. The observed effects of ultrasound on the introduced gas slugs (left side of each frame). Without ultrasound (silent) the hemispherical interface remained undisturbed. With ultrasound at 47 kHz surface wave oscillations set in on the interface. At 411 and 601 kHz the hemispherical interfaces became deformed and fine liquid droplets were dispersed into the gas slugs. High-speed video recordings of these effects can be found in the ESI, see Vid. 1 and Vid. 2.

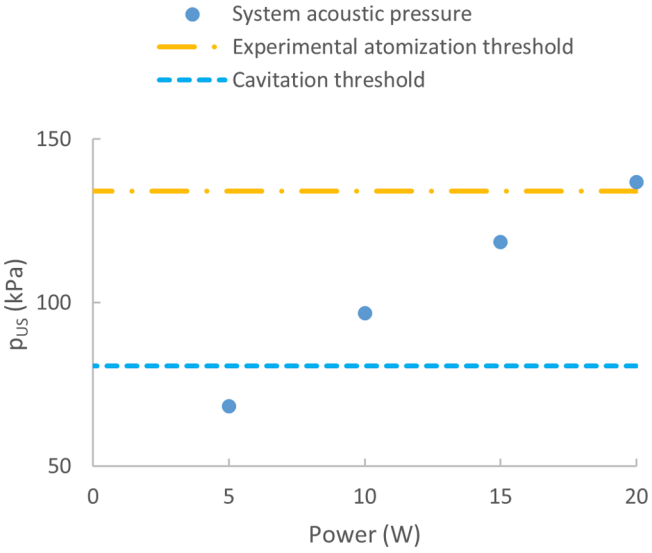

Fig. 4. The system acoustic pressures for the silicone etched reactor with increasing power compared to the pressure thresholds found in literature.

2.4. Acoustic simulations

The surface displacement of the piezo at 411.8 kHz, illustrated in Fig. 2 was used as the input displacement condition to determine the sound field inside the channels using the pressure acoustics (frequency domain) module without any attenuation; the assumption is that the bottom surface of the channels is in contact with the piezo, neglecting the glue layer, see overlay in Fig. 2. This was done using a "general extrusion" which maps the displacement from the piezoelectric transducer into the "normal displacement" node in the pressure acoustics module. Then the Helmholtz equation is solved for this study

$$\nabla^2 P - k^2 P = 0 \tag{5}$$

where P is the pressure (Pa) and $k = \omega/c$ is the wave number and c the speed of sound.

The channels are comprised of alternating gas (air) and liquid (water) segments. To simplify the calculation, the silicone walls and glass cover were not modelled. Instead, the channel walls were modelled as sound hard while the ends of the channels as sound soft. We refer to the ESI section S2 for the procedure and numerical admittance curves.

An electric potential of only 1 V was applied to determine the sound fields inside the channels for the numerical studies. This is much lower than the actual potential applied to the transducer which ranged up to 15 V (amplitude) for the experiments, since realistic potentials led to apparently too high and unrealistic pressure predictions. This might occur because acoustic damping is neglected in the Helmholtz

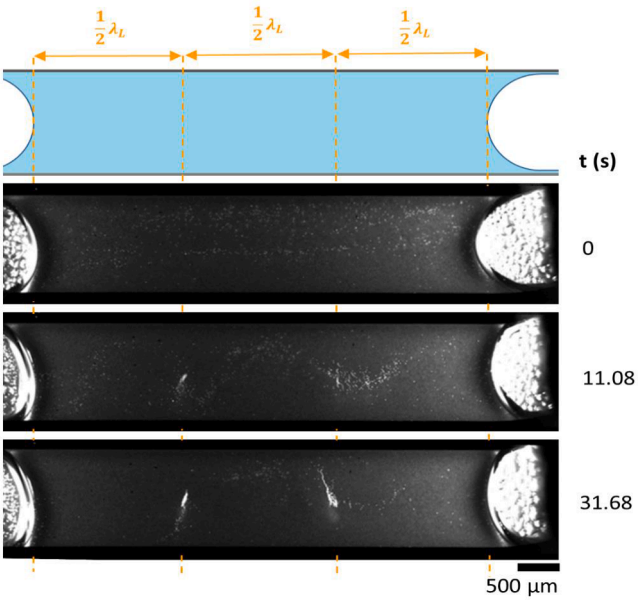

Fig. 5. Particles suspended in a liquid slug between two gas bubbles inside a microfluidic channel under stagnant conditions. With ultrasound on, the particles accumulated at distances of $1/2\lambda_L$ within the liquid slug, indicating the pressure nodes of the standing wave formed within the slug. The liquid slug length approximately matched $3/2\lambda_L$ and four nodes were formed, two at the gas–liquid interfaces and two in the bulk of the slug. The images have been sharpened to accentuate the particles within the channel. On the right of each frame the elapsed time since ultrasound was turned on is indicated.

simulation and boundary conditions are fully reflective (sound hard), which is partly unrealistic. Additional damping by the silicone, glass plate and glue layer is neglected as well. Furthermore, the resonance condition might not have been fully met in the experiments and/or might have been limited by nonlinear effects that are not included in the simulation. Therefore, the absolute acoustic pressures determined by COMSOL should only be regarded as qualitative, while the spatial distribution appears reasonable.

3. Results and discussion

3.1. Effects of ultrasound on the gas bubbles in gas–liquid segmented flow

In Fig. 3, the observed effects of ultrasound on the gas–liquid interface of the introduced gas slugs at the silicone etched reactor's resonant frequencies. At 47 kHz surface wave oscillation was observed with a capillary wavelength of 62 ± 3 µm, which corresponded well with the theoretical capillary wavelength (λ_c = 59 µm) according to Kelvin's equation [32,33]:

$$\lambda_c = \left(\frac{2\pi\sigma}{\rho f_c^2}\right)^{\frac{1}{3}} \tag{6}$$

Here, σ denotes the interfacial tension, ρ the liquid density and f_c the frequency of the free surface capillary waves which equalled the driving frequency (f) for this system. At 411 and 601 kHz, however, significant interface deformation along with large amounts of dispersed liquid droplets inside the gas slugs were observed. The dispersion of a bulk liquid into a fine mist with ultrasound, commonly referred to as atomization, has been studied in detail for unconfined systems over the years [34–38], however, reports of atomization in the confined space of a microfluidic channel are more scarce [39,40], indicating relatively high ultrasonic driving powers. The definition of applied ultrasonic power can be somewhat ambiguous for systems at different scales, making it difficult to compare the powers directly. For this reason, direct comparisons are made with more recent systems operating at similar conditions and at a similar scale. Keeping this in mind, ultrasonic atomization and bubble deformation to the extent shown here has not been previously reported for similar gas–liquid systems in Taylor flow. The images were captured at a load power of 15 W with a liquid and gas flow rate of 1 ml/min and 1.5 ml/min respectively.

According to Pohlman *et al.* [41,42], the threshold at which atomization would occur at a driving frequency f can be described by:

$$A_t = \frac{4\mu}{\rho f \lambda_c} \tag{7}$$

with A_t the critical oscillation amplitude of capillary waves for surface instability and μ the viscosity of the liquid. Combining Eqs. (6) and (7)

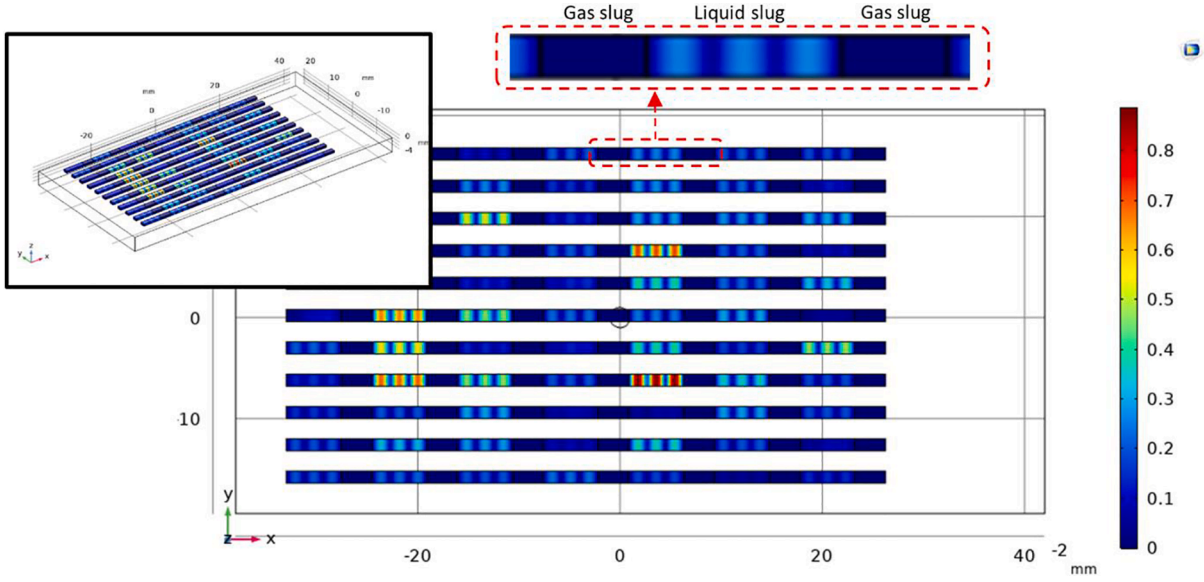

Fig. 6. Absolute acoustic pressure inside the reactor channels for a slug length of $3/2\lambda_L$. The gas bubbles are depicted by the dark blue regions and are set at a length of 3 mm, the coloured regions adjacent to gas slugs are the liquid slugs with a length of 5.46 mm as indicated by the magnified insert above. The overlay to the left depicts a 3D view of the channels and the unit of the colour-bar is in bar. Note that the simulated pressure magnitude does not necessarily represent the actual pressure magnitude inside the channels. (For interpretation of the references to colour in this figure legend, the reader is referred to the web version of this article.)

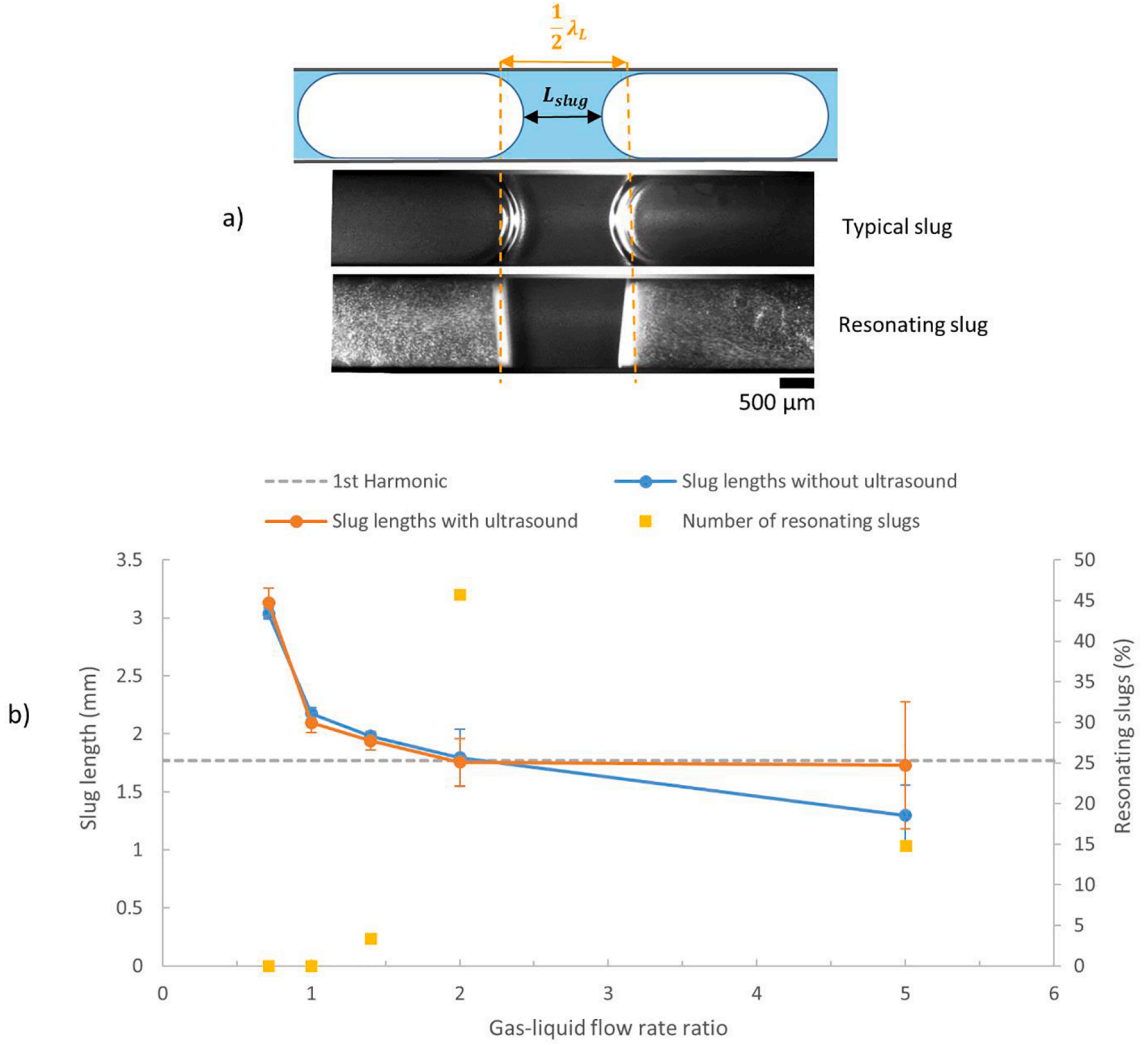

Fig. 7. a) A typical liquid slug and a "resonating" liquid slug in gas–liquid Taylor flow. b) Effect of liquid slug length on resonance and atomization. On the primary axis, the measured liquid slug lengths with and without ultrasound, and on the secondary axis the amount of "resonating" slugs expressed as a number percentage. Recordings for both silent and sonicated conditions for a gas–liquid flow rate ratio of 2 can be found in the ESI, see Vid. 5 and Vid. 6.

results in a linear relation between A_t and $f^{-\left(\frac{1}{3}\right)}$. Assuming the surface oscillation amplitude scales linearly with the acoustic velocity amplitude, which in turn scales with the square root of the acoustic power [22] the threshold power for atomization would scale with $f^{-\left(\frac{2}{3}\right)}$. According to this relation, the threshold power for 47 kHz is about 4.2 times that for 411 kHz. Therefore, this analysis supports a reduced atomization power threshold at higher frequencies, but cannot quantitatively account for the observation that for 411 kHz atomization was observed at load powers as low as 5 W whereas, for 47 kHz, no atomization was observed at load powers up to 30 W. Similarly, load powers were reportedly increased up to 50 W for similar systems operating at 20 and 40 kHz with little to no atomization observed [22,23]. This indicates that atomization is caused by an additional effect for this system. The expected acoustic pressures of the silicone etched microreactor were compared to the typical pressure thresholds required for atomization and cavitation found in literature. Here the acoustic pressure amplitude $p_{US} = \sqrt{(2I_p \rho c_s)}$ for the system was calculated from the spatially averaged ultrasound intensity $I_p = Power/Area$, based on a plane wave assumption, which is typically used in ultrasonic research. As shown in Fig. 4, the acoustic pressures were above the cavitation threshold [43] and slightly below the atomization threshold for thin film atomizers operating at 500 kHz [44].

A second argument that atomization for this system is caused by an additional effect can be derived from the observation that only a portion of the introduced gas slugs was experiencing spray injection. It was found that gas slugs adjacent to liquid slugs whose length matched approximately an integer of half the wavelength of ultrasound in water ($n/2\lambda_L$, $n = 1, 2, 3, 4, 5$) were undergoing atomization and interface deformation, as shown in Fig. S6 in the ESI.

For the silicone etched reactor operating at 601 kHz interface deformation would become, on occasion, so severe that a single gas slug would split into two as depicted in Fig. S6 e), a high-speed video recording of this effect can be found in the ESI, see Vid. 2. The exact cause of this deformation is unclear at this stage, a possible cause might be acoustic resonance, which is discussed in Section 3.2, coupled with the effects of acoustic cavitation.

3.2. Resonance in the liquid slug

The dependence of atomization on the liquid slug length indicates that atomization could be caused by resonance within the liquid slugs. Suspended particles and droplets migrate towards the pressure nodes or antinodes of a standing wave, depending on the properties of the ma-

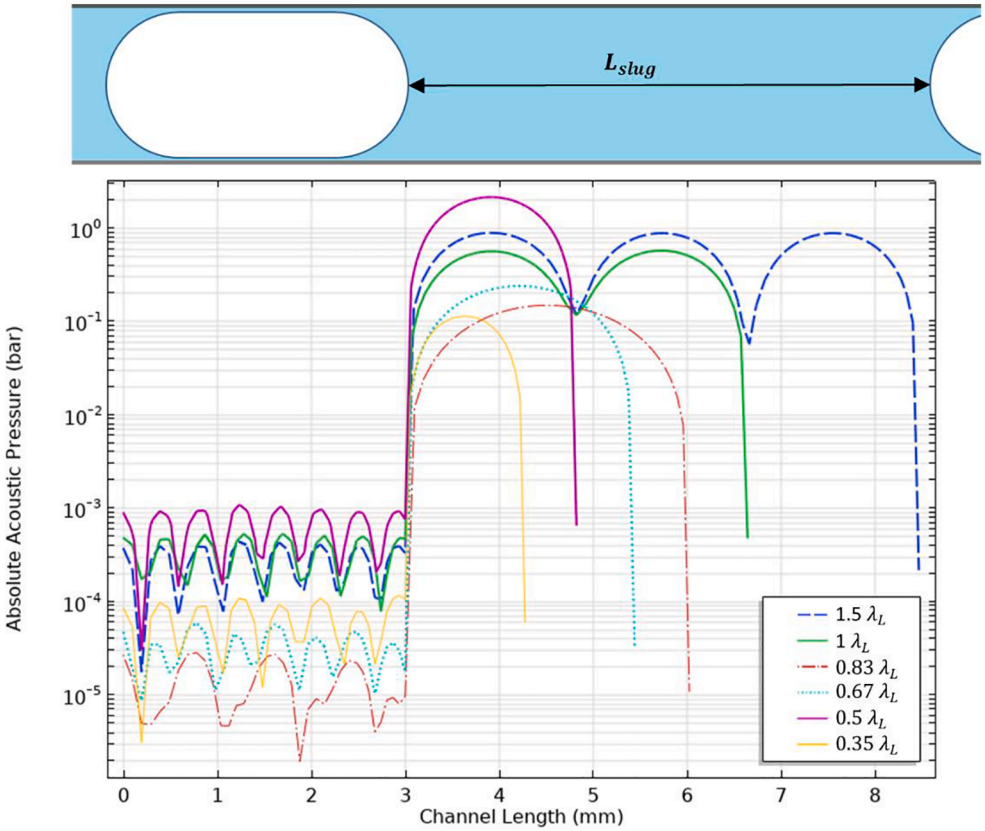

Fig. 8. Predicted absolute acoustic pressures with slug length. The first three millimetres of the channel length represents the gas bubble and thereafter the liquid slug at the different lengths expressed in terms of λ_L.

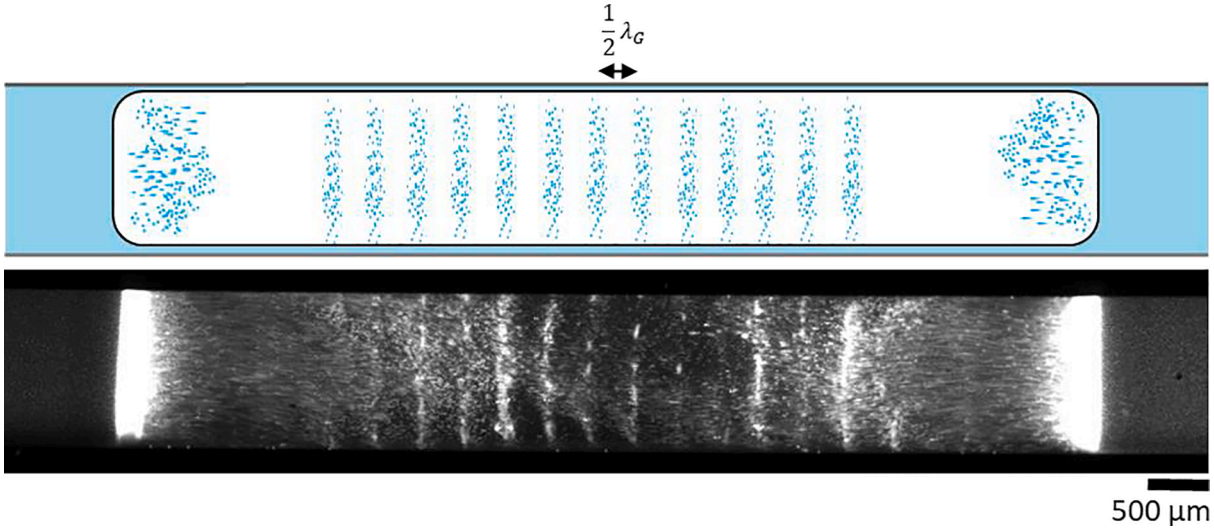

Fig. 9. Experimental image and schematic illustration of resonance within a gas bubble at 411 kHz.

terial. Solid particles generally have a positive contrast factor and move towards the pressure nodes [16]. To determine if resonance is occurring within liquid slugs, inert polystyrene particles (1 wt%, 10 µm, Sphero-tech) were suspended in the liquid phase. Once stable gas–liquid Taylor flow was established, both the gas and liquid flow was stopped and ultrasound was applied at a frequency of 411 kHz and a reduced power of 10 W to attenuate the effects of cavitation microstreaming. For a portion of the liquid slugs, particles indeed migrated and gathered at intervals of 1.82 ± 0.36 mm or approximately $1/2\lambda_L$ from each other, as depicted in Fig. 5, indicating the pressure nodes of the standing wave formed within the liquid slugs. A second experiment was carried out with a small amount of pressure applied on the liquid feed syringe to induce creep flow. Particles would focus at the pressure nodes as in the previous experiment and stay focused at these positions while slowly moving along with the liquid slug, indicating that resonance is established within the liquid slugs and not only the reactor. Video recordings for both the stop and creep flow experiments can be found in the ESI, see Vid. 3 and Vid. 4.

The sound field inside the reactor channels for the liquid slug in the stop-flow experiment (Fig. 5) was determined using COMSOL. The gas

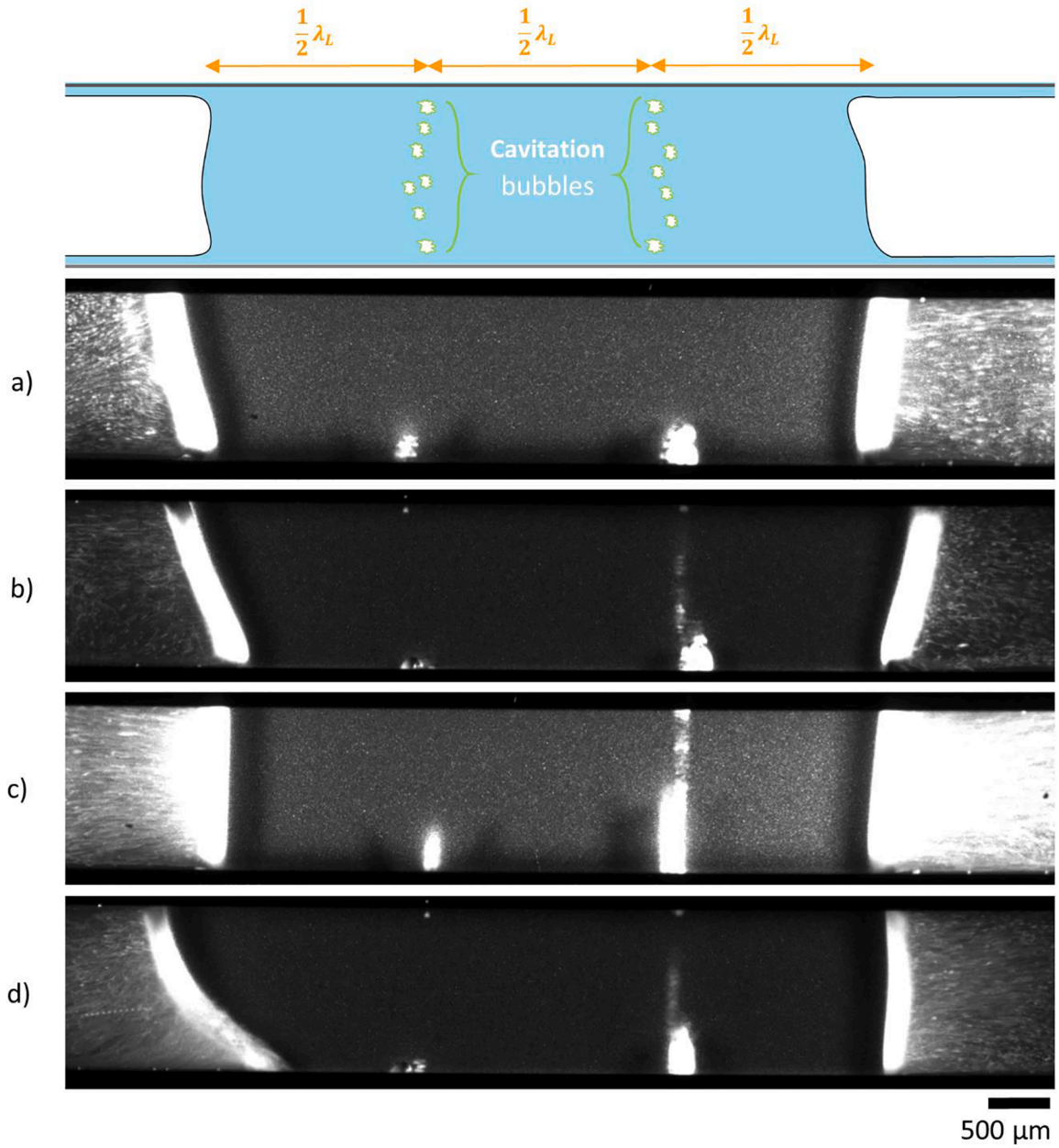

Fig. 10. Cavitation bubbles located at the suspected pressure nodes of the liquid slug at 411 kHz. In a) and b) atomization is not occurring and the cavitation bubbles that are not violently oscillating. In c) and d) atomization is occurring and the cavitation bubbles are violently oscillating. The high-speed video recording can be found in the ESI, see Vid. 8.

bubble lengths were kept constant at 3 mm and the liquid slug lengths were set to 5.46 mm or $3/2\lambda_L$. At a frequency of 411.8 kHz a standing wave pattern is seen to develop inside the liquid slugs, see Fig. 6, with two pressure nodes located at the gas–liquid interfaces and two in the bulk of the slugs as indicated by the focussed particles in Fig. 5. What is also apparent from Fig. 6 is that the spatial distribution of the acoustic pressure along the reactor channels is not uniform, most likely caused by the spatial variability of the transducer's excitation. The influence of the acoustic spatial distribution won't be discussed in detail here, but it is an important aspect when designing and characterising these types of reactors for microfluidic applications, for which numerical simulations such as these can serve as a useful tool.

To provide further evidence on the link between atomization and resonance the effect of gas-liquid flow rate ratio (q_G/q_L), i.e. slug length (L_{slug}) [45], on the likelihood of atomization was investigated. For a total flow rate of 1.2 ml/min the gas–liquid flow rate ratio was increased and the liquid slug lengths measured from bubble cap to cap with and without ultrasound applied at 411 kHz and 15 W. Furthermore, the number of "resonating" slugs, i.e. liquid slugs with severe atomization occurring in the adjacent gas bubbles, were counted, see Fig. 7a). These measurements were taken at a fixed position, 50 mm along the first channel, where previous experiments indicated strong ultrasonic effects and more than 60 liquid slugs in total were considered for each condition.

The results, depicted in Fig. 7b), show that for a gas–liquid flow rate ratio of 2 the slug length approximately matched the first harmonic, i.e. $1/2\ \lambda_L$, and that the number of "resonating" slugs, 45% in total, was significantly higher than at the other ratios. Secondly, for the higher gas–liquid flow rate ratio ultrasound resulted in an overall increase in the liquid slug length when compared with non-sonicated conditions. Thirdly, the measured length of the "resonating slugs" remained unchanged regardless of the gas–liquid flow rate ratio, with an average

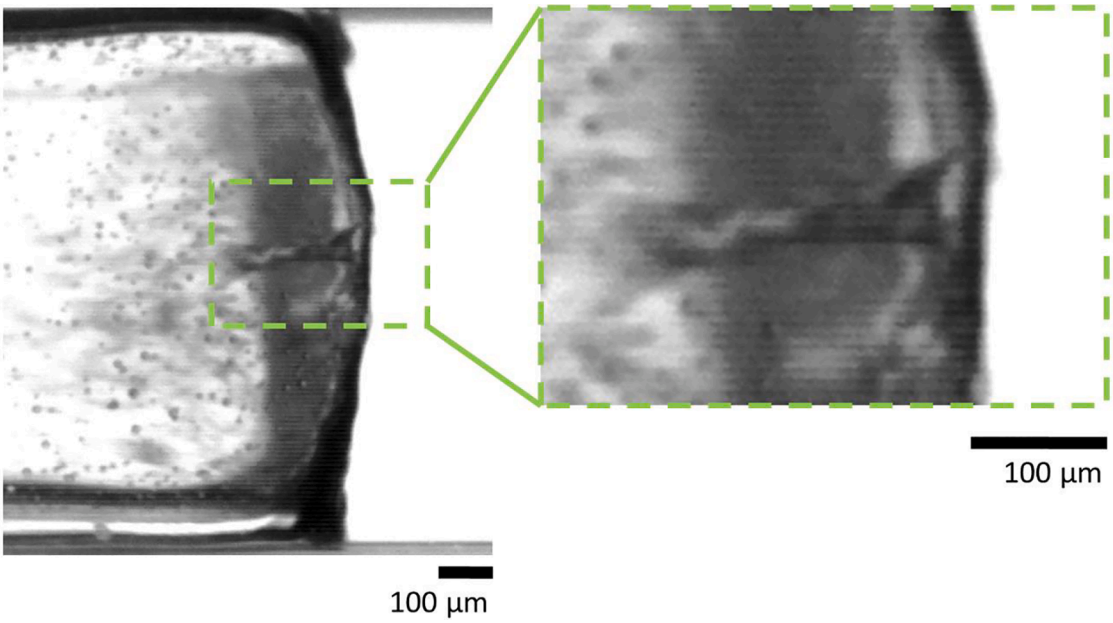

Fig. 11. Cavitation bubble directly leading to atomization at 439 kHz and 5 W, enlarged insert on the right depicts the liquid fountain type of droplet ejection typically associated with the cavitation hypothesis. The high-speed video recording of this event can be found in the ESI, see Vid. 9.

length of 1.64 ± 0.02 mm or approximately $1/2\lambda_L$. The exact cause for the increased slug length is at this stage unknown, a potential explanation could be related to primary Bjerknes forces [46,47].

The sound field inside reactor channels for the measured slug lengths as well as for slug lengths at higher harmonics was determined using COMSOL. Fig. 8 compares the simulated absolute acoustic pressures for the different slug lengths for a single gas bubble and liquid slug at the centre of the reactor. For slugs matching a multiple of $1/2\lambda_L$ there are clear nodes and antinodes formed within the liquid slug with an order of magnitude increase in the acoustic pressures at the antinodes when compared to slugs without strong resonance. Note that the magnitude of the predicted acoustic pressures does not represent the actual acoustic pressures magnitude inside the channels, and should only be considered qualitatively indicating the relative pressure increase as well as the locations of the nodes and antinodes for the different slug lengths.

In addition to slug resonance there appeared to be resonance within the gas bubble, this was experimentally also observed. Fig. 9 depicts a single gas bubble where atomization is occurring from both the left and the right interface, the dispersed droplets in the gas bubble then gathered at planes at a distance of 0.34 ± 0.03 mm or approximately $\frac{1}{2}\lambda_G$ from each other. The dispersed droplets would then coalesce at these planes to form larger droplets and eventually merge with the gas–liquid interface. The image was taken at 411 kHz, 15 W and a liquid–gas flow rate of 2 and 4 ml/min respectively.

3.3. Mechanism of acoustic atomization

At this stage, the exact cause of atomization observed in gas bubbles adjacent to resonating slugs is unclear. The increased acoustic pressure resulting from resonance could explain the presence of atomization as the atomization threshold is exceeded. In addition, from Fig. 10 and the footage (Vid. 1) given in the ESI, it is clear that cavitation bubbles other than the introduced gas phase are present in the system and could act as a possible source for atomization. Whether these cavitation bubbles originate from dissolved gas in the liquid phase or are the result of bubble pinch off from capillary waves [26,40] could not be determined, as higher frame rates were required to observe the oscillation behaviour of capillary waves at these driving frequencies. Nonetheless, their size, position and oscillation behaviour could be determined. In Fig. 10 cavitation bubbles larger than the linear resonance radius (R_r = 6.83 µm) were located at the suspected pressure nodes within the liquid slug.

$$R_r = \frac{1}{2\pi f}\sqrt{\frac{3\gamma P_h}{\rho}} \tag{8}$$

With $\gamma = c_p/c_v$ the ratio of the specific heat of the gas at constant pressure over the specific heat of the gas at constant volume and P_h the hydrostatic liquid pressure. One can therefore deduce that cavitation bubbles larger than R_r would also be present at the pressure nodes located at the interface of the gas bubbles. However, these cavitation bubbles were secluded by the interface. The presence of cavitation bubbles at the gas–liquid interface was confirmed though using the more visibly accessible glass capillary reactor, see Fig. S7 and Vid. 7 in the ESI.

Cavitation bubbles at pressure nodes would not be expected to violently oscillate as the driving pressure at the nodes would be low. This was the case when atomization was not occurring, see Fig. 10 a) and b). However, when atomization did occur these cavitation bubbles would be violently oscillating, see Fig. 10 c) and d). The cavitation bubbles located at the gas–liquid interface could possibly interact with the interface and cause atomization. The violent oscillation of the cavitation bubbles at the nodes could be due to the fluctuating acoustic field within the liquid slug caused by the dynamic behaviour of the gas–liquid interface of the gas slugs acting as the reflective plane.

Since ultrasound was first used to break up bulk liquids into fine mists of small droplets the mechanisms behind ultrasonic atomization were not well understood [35]. From the first observations it was clear that the two effects of ultrasound, viz. capillary waves and cavitation, play a significant and possibly coupled role [36]. And today there is still debate between three major hypotheses about the mechanism, viz. the *capillary wave hypothesis*, the *cavitation hypothesis* and *conjunction theory*. An important aspect when considering the mechanisms mentioned is the methods used to generate atomization, as there are substantial differences in the nature and mechanics of different atomizers [37].

The *capillary-wave hypothesis* states that aerosol droplets are formed at the crests of capillary waves due to an onset of surface instability at the interface. For the atomization of thin liquid films at low frequency ultrasound [48] as well for more recent Surface Acoustic Wave (SAW) atomizers operating at higher frequencies [33] the existence of a constant relationship between the mean aerosol diameter ($\overline{D}$) and capillary

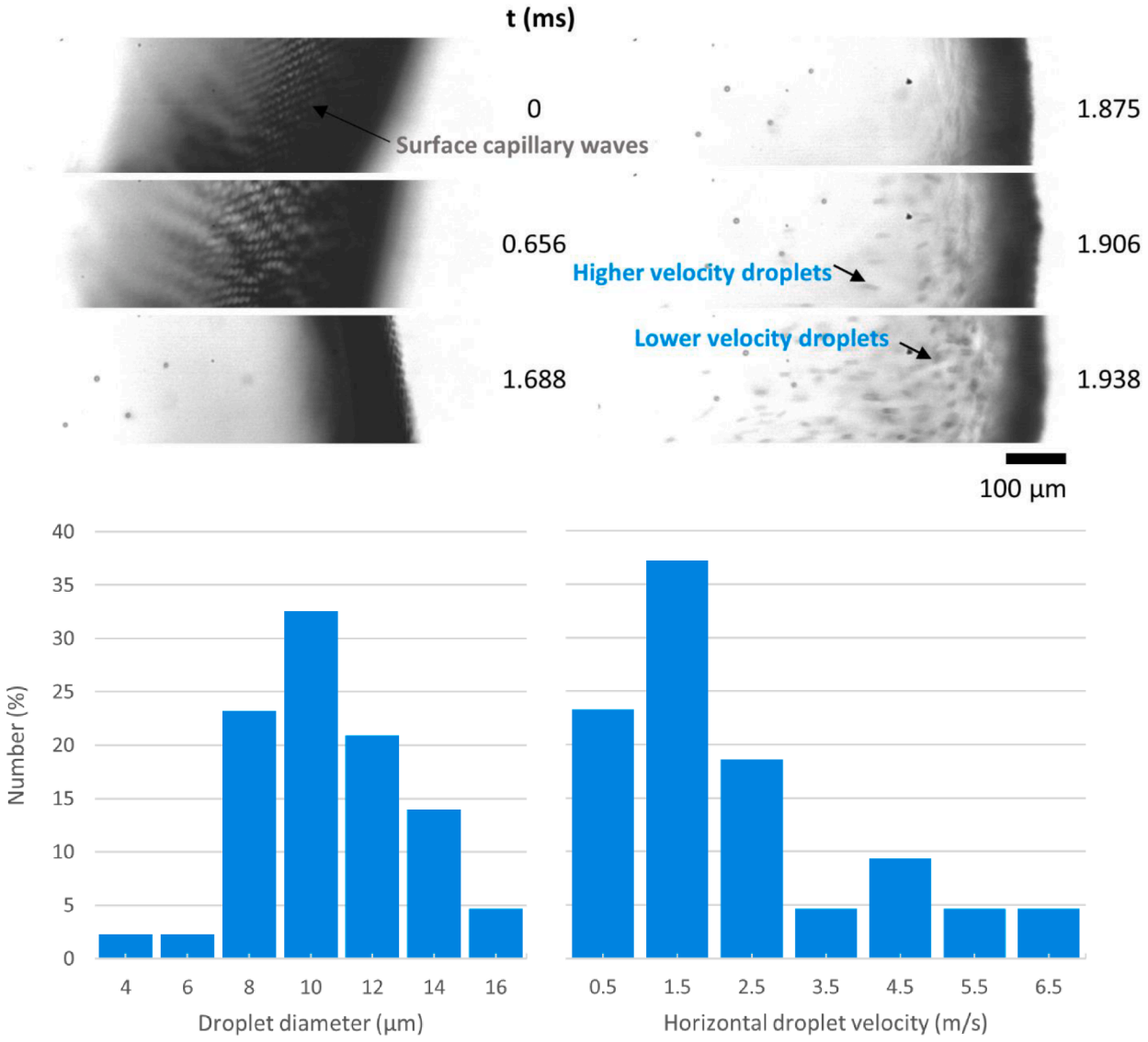

Fig. 12. Capillary waves and atomization occurring at 439 kHz and 5 W as well as the size distribution and velocity profile of the ejected droplets.

wavelength (λ_C) is sound evidence in support of this hypothesis and forms one of the fundamental principles of acoustic atomization:

$$\overline{D} = \alpha\lambda_C \tag{9}$$

with α independent of the acoustic frequency. However, the frequent occurrence of large liquid fountains and jets that burst into smaller droplets during sonication has also led to the development and support of the *cavitation hypothesis* [35,49,50]. According to this hypothesis, cavitation plays a direct role, i.e. hydraulic shocks generated by collapsing cavitation bubbles near a gas–liquid interface rupture it to form the aerosol droplets. This has led to extensive investigations into the atomization of liquid fountains produced by directing high-intensity high-frequency ultrasound from the depth of a liquid to its surface. The emission of sonoluminescence during an atomization event as well as an increase of atomization threshold with elevated pressures and prior degassing provide ample evidence to support the role of cavitation [36], be it direct or indirect. Finally, these observations lead to the *conjunction theory*, also referred to as the *cavitation-wave hypothesis*, which states that the periodic hydraulic shocks from cavitation bubbles do not only cause atomization directly but also excite the finite amplitude capillary waves which then lead to the ejection of aerosol droplets, i.e. cavitation plays an indirect role.

In Fig. 11 the collapse of a cavitation bubble near the gas–liquid interface can be seen ejecting liquid droplets into the gas bubble at very high velocities, up to 7.58 ± 1.35 m/s. However, cavitation collapse directly leading to atomization was not always observed and was not necessarily the prevailing mechanism.

In most atomization events, prior to the ejection of droplets, capillary waves were visible on the interface, as depicted in Fig. 12 at time t = 0 to 1.688 ms. The measured wavelength (14.31 ± 1.04 µm) corresponds well with theoretical wavelength (λ_c) according to Eq. (6). Here the frequency of the free surface capillary waves was set equal to the driving frequency of 439 kHz. However, right before the onset of atomization at t = 1.875 ms, the interface became distorted and capillary waves were near impossible to distinguish. Therefore, the ejected droplet velocities and diameters were measured directly after atomization had occurred, as to prevent the influence of recirculating and merged droplets. The droplet velocities were estimated by tracking droplets between subsequent frames and measuring the distance travelled multiplied by the frame rate at which the recordings were taken (32,000 fps), this was done for 44 droplets over a series of 9 atomization events. The results are depicted in Fig. 12. From the distributions it is clear that the majority of droplet diameters are smaller than the capillary wavelength as per the capillary-wave hypothesis. However, the presence of droplets larger

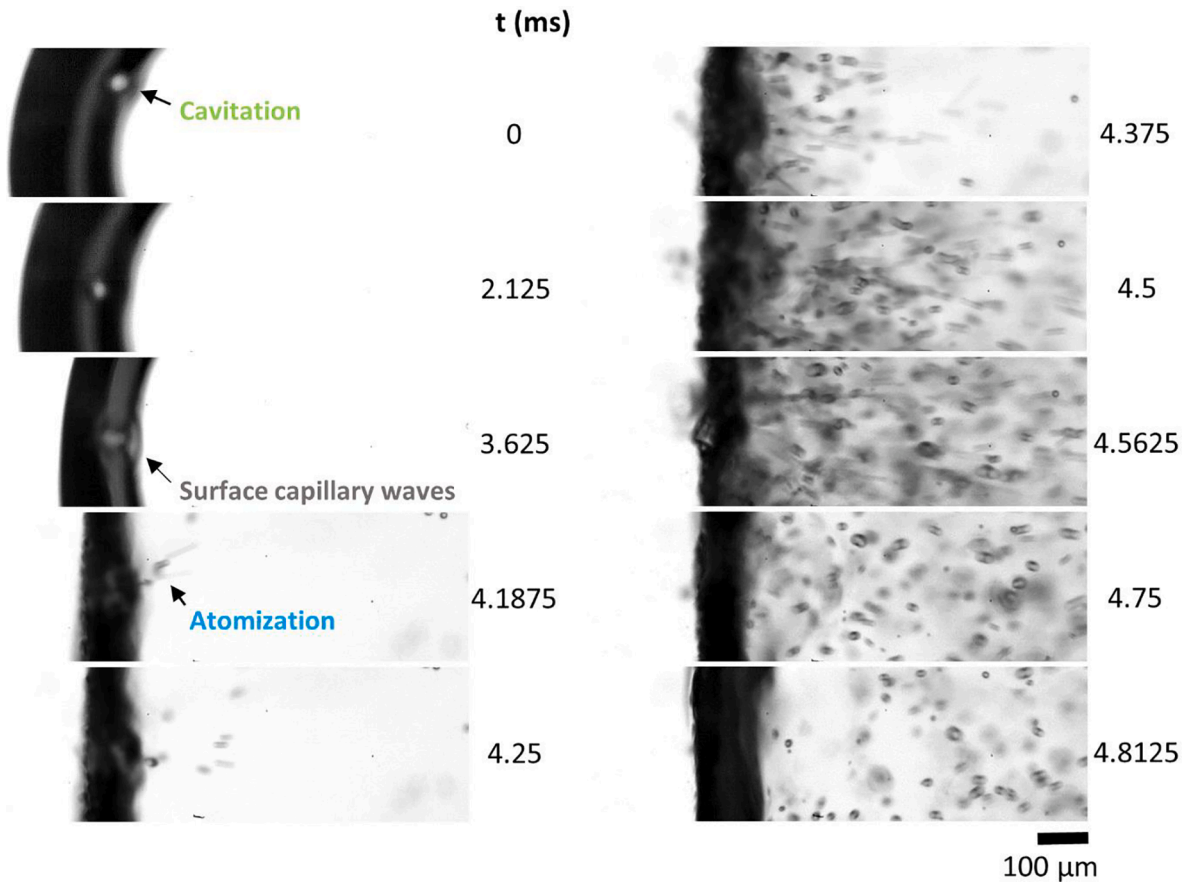

Fig. 13. Oscillating cavitation bubble leading towards atomization at 156.5 kHz and 5 W. The first three frames have been brightened to accentuate the cavitation bubble at the gas–liquid interface.

than the capillary wavelength and the high ejection velocities suggest that cavitation could play a role [51,52]. From the experimental footage, it was also observed that the higher velocity droplets (4.5 m/s) were for most cases followed by a larger amount of lower velocity droplets (1.5 m/s).

For the experiments carried out at lower frequencies, 156.5 kHz and 86.5 kHz, the larger cavitation bubbles became more discernible at the gas–liquid interface. These cavitation bubbles were seen migrating towards the gas–liquid interfaces where they would, on occurrence, violently oscillate resulting in the ejection of droplets into the gas phase. Operating at 156.5 kHz, Fig. 13 depicts a cavitation bubble oscillating near the gas–liquid interface, at 4.1875 ms violent oscillations result in the ejection of droplets into the gas bubble. Similarly, operating at 86.5 kHz, Fig. 14 depicts an oscillating cavitation bubble migrating towards the gas–liquid interface where, at 4.625 ms, droplets are being ejected in the vicinity of the cavitation bubble. Video recordings taken at a higher magnification, depicted by the insert of Fig. 14, showed that cavitation bubbles were inducing capillary waves on the surface of the interface. Video recordings of these effects can be found in the ESI, see Vid. 10, Vid. 11 and Vid. 12.

Based on the above observations one can propose that the transient oscillating behaviour of cavitation bubbles near the gas–liquid interface of the introduced gas bubbles is the primary cause of atomization for this system. One can go further as to say that atomization is more likely when the liquid slugs are in a state of resonance as pressure nodes are formed at the gas–liquid interfaces, which cavitation bubbles larger than R_r migrate towards. The increased cavitational activity in the vicinity of the gas–liquid interface coupled with the dynamic acoustic field within the liquid slug causes by the gas–liquid interface acting as a reflective plane would explain the transient atomization behaviour observed in this system.

The capillary wave constant (α) for the confined systems was compared to that of unconfined atomizers. This was done by taking the average size of the atomized droplets for the different operating frequencies and dividing it by the corresponding capillary wavelength according to Eq. (6). The results depicted in Fig. S8 in the ESI estimates a α of 0.71, which is larger than the typical values found in literature [48,50,53] for thin film atomizers operating at similar frequency ranges for similar working fluids, see Table S1 in the ESI. A possible explanation for the larger droplet sizes could be due to the role cavitation plays on atomization observed for the confined channels.

4. Conclusions

We have shown how a liquid slug in gas–liquid segmented flow can act as an acoustic resonator and investigated the link between this phenomenon and the extensive atomization observed within the microchannels. This was done by utilizing the confined space of the microchannel to study the mechanisms of atomization, providing, to the best of our knowledge, visual evidence of the *cavitation-wave hypothesis* for the first time. Atomization of this extent occurring during gas–liquid segmented flow increases the interfacial area between the two phases considerably, which can be utilized for processes limited by gas–liquid mass transfer and/or phase distribution within microchannels.

In summary, strong acoustic resonance within a liquid slug was observed when the measured length of the liquid slug was within a harmonic of the driving ultrasonic frequency. As a result, pressure nodes and antinodes were formed within the liquid slug. Numerical simulations indicated an order of magnitude increase in the absolute acoustic pressure at the pressure antinodes when a liquid slug was in a state of

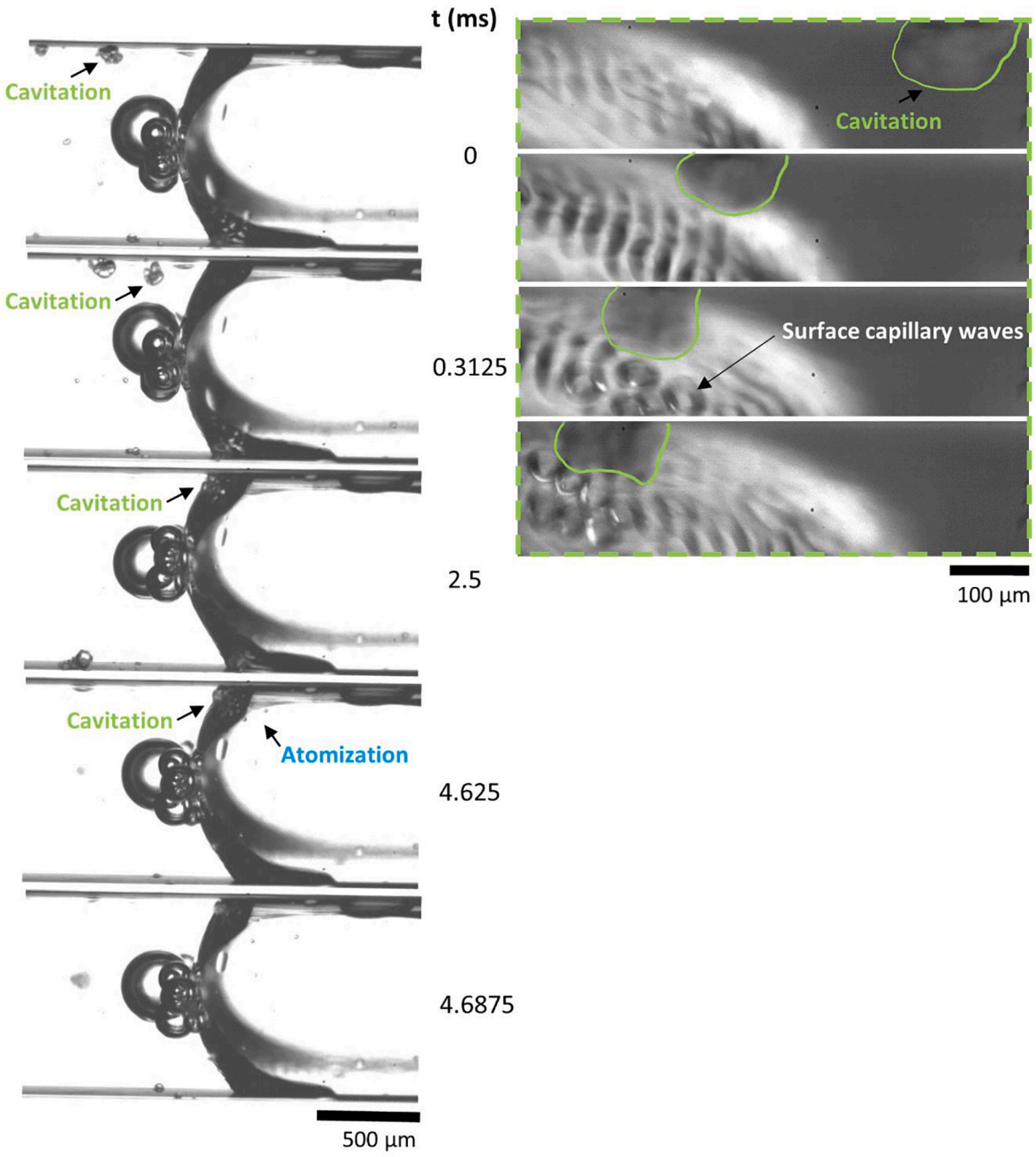

Fig. 14. Oscillating cavitation bubble leading towards atomization at 86.5 kHz and 5 W. Insert on the right depicts an oscillating cavitation bubble inducing capillary waves on the gas-liquid interface.

resonance. Resonance within the liquid slugs also appeared to have an effect on the phase distribution within the reactor channels, however, a conclusion as to the cause of the distribution could not be made and is subject to future work. The link between resonance within the slugs and the observed atomization appeared to be due to the distribution of cavitation bubbles within the slug. At a state of resonance cavitation bubbles were observed in the vicinity of the interface of the gas bubbles where they would interact with the interface to eject droplets. The most common interaction of the cavitation bubbles with the gas–liquid interface appeared to be in coherence with the cavitation-wave mechanism. Although, the capillary wave mechanism could not be ruled out and is likely to play a role due to the larger acoustic pressures observed at resonance. Future applications of the observed phenomena could include the use of atomization to increase interfacial area between the gas and liquid phase, speeding up reactions that are limited either by mass transfer and/or phase distribution. Secondly, resonance within microchannels has the possibility to increase the efficiency of ultrasound used for clogging prevention, emulsification and particle size reduction in microreactors.

Declaration of Competing Interest

The authors declare that they have no known competing financial interests or personal relationships that could have appeared to influence the work reported in this paper.

Acknowledgements

This project has received funding from the European Research Council (ERC) under the European Union's Horizon 2020 research and

innovation programme (grant agreement No. 101001024). Z.D. acknowledges funding from Chemistry and Chemical Engineering Guangdong Laboratory (Grant No. 2011009). D. S. and R. M. acknowledge funding from the European Union's Horizon 2020 research and innovation programme under the Marie Skłodowska-Curie grant agreement No 721290 (MSCA-ETN COSMIC).

Appendix A. Supplementary data

Supplementary data to this article can be found online at https://doi.org/10.1016/j.ultsonch.2021.105611.

References

[1] K. Jähnisch, V. Hessel, H. Löwe, M. Baerns, Chemistry in microstructured reactors, Angew. Chemie - Int. Ed. 43 (4) (2004) 406–446, https://doi.org/10.1002/anie.200300577.
[2] A. Müller, V. Cominos, V. Hessel, B. Horn, J. Schürer, A. Ziogas, K. Jähnisch, V. Hillmann, V. Großer, K.A. Jam, A. Bazzanella, G. Rinke, M. Kraut, Fluidic bus system for chemical process engineering in the laboratory and for small-scale production, Chem. Eng. J. 107 (2005) 205–214, https://doi.org/10.1016/j.cej.2004.12.030.
[3] T. Inoue, M.A. Schmidt, K.F. Jensen, Microfabricated multiphase reactors for the direct synthesis of hydrogen peroxide from hydrogen and oxygen, Ind. Eng. Chem. Res. 46 (4) (2007) 1153–1160, https://doi.org/10.1021/ie061277w.
[4] R. Hartman, J. Naber, S. Buchwald, K. Jensen, Multistep microchemical synthesis enabled by microfluidic distillation, Angew. Chemie - Int. Ed. 49 (5) (2010) 899–903, https://doi.org/10.1002/anie.200904634.
[5] A.K. Liedtke, F. Bornette, R. Philippe, C. De Bellefon, Gas-liquid-solid "slurry Taylor" flow: experimental evaluation through the catalytic hydrogenation of 3-methyl-1-pentyn-3-ol, Chem. Eng. J. 227 (2013) 174–181, https://doi.org/10.1016/j.cej.2012.07.100.
[6] F. Lévesque, P.H. Seeberger, Highly efficient continuous flow reactions using singlet oxygen as a "Green" reagent, Org. Lett. 13 (19) (2011) 5008–5011, https://doi.org/10.1021/ol2017643.
[7] J. Zhang, K. Wang, A.R. Teixeira, K.F. Jensen, G. Luo, Design and scaling up of microchemical systems: A review, Annu. Rev. Chem. Biomol. Eng. 8 (1) (2017) 285–305, https://doi.org/10.1146/annurev-chembioeng-060816-101443.
[8] I. Rossetti, M. Compagnoni, Chemical reaction engineering, process design and scale-up issues at the frontier of synthesis: flow chemistry, Chem. Eng. J. 296 (2016) 56–70, https://doi.org/10.1016/j.cej.2016.02.119.
[9] V. Hessel, D. Kralisch, N. Kockmann, T. Noël, Q.i. Wang, Novel process windows for enabling, accelerating, and uplifting flow chemistry, ChemSusChem. 6 (5) (2013) 746–789, https://doi.org/10.1002/cssc.v6.510.1002/cssc.201200766.
[10] D. Fernandez Rivas, S. Kuhn, Synergy of microfluidics and ultrasound: process intensification challenges and opportunities, Top. Curr. Chem. 374 (2016) 1–30, https://doi.org/10.1007/s41061-016-0070-y.
[11] D. Fernandez Rivas, P. Cintas, H.J.G.E. Gardeniers, Merging microfluidics and sonochemistry: towards greener and more efficient micro-sono-reactors, Chem. Commun. 48 (2012) 10935–10947, https://doi.org/10.1039/c2cc33920j.
[12] S. Hübner, S. Kressirer, D. Kralisch, C. Bludszuweit-Philipp, K. Lukow, I. Jänich, A. Schilling, H. Hieronymus, C. Liebner, K. Jähnisch, Ultrasound and microstructures-a promising combination? ChemSusChem 5 (2) (2012) 279–288, https://doi.org/10.1002/cssc.201100369.
[13] Z. Dong, S. Kuhn, C. Delacour, K. Mc Carogher, P.U. Aniket, Continuous ultrasonic reactors: design, Mech. Appl., Mater. (Basel) 13 (2020).
[14] S. Kuhn, T. Noël, L. Gu, P.L. Heider, K.F. Jensen, A Teflon microreactor with integrated piezoelectric actuator to handle solid forming reactions, Lab Chip. 11 (2011) 2488–2492, https://doi.org/10.1039/c1lc20337a.
[15] Z. Dong, D. Fernandez Rivas, S. Kuhn, Acoustophoretic focusing effects on particle synthesis and clogging in microreactors, Lab Chip. 19 (2) (2019) 316–327, https://doi.org/10.1039/C8LC00675J.
[16] F.J. Trujillo, P. Juliano, G. Barbosa-Cánovas, K. Knoerzer, Separation of suspensions and emulsions via ultrasonic standing waves - a review, Ultrason. Sonochem. 21 (6) (2014) 2151–2164, https://doi.org/10.1016/j.ultsonch.2014.02.016.
[17] Z. Dong, A.P. Udepurkar, S. Kuhn, Synergistic effects of the alternating application of low and high frequency ultrasound for particle synthesis in microreactors, Ultrason. - Sonochem. 60 (2020) 104800, https://doi.org/10.1016/j.ultsonch.2019.104800.
[18] J.J. John, S. Kuhn, L. Braeken, T. Van Gerven, Ultrasound assisted liquid–liquid extraction with a novel interval-contact reactor, Chem. Eng. Process. Process Intensif. 113 (2017) 35–41, https://doi.org/10.1016/j.cep.2016.09.008.
[19] D. Rossi, R. Jamshidi, N. Saffari, S. Kuhn, A. Gavriilidis, L. Mazzei, Continuous-flow sonocrystallization in droplet-based microfluidics, Cryst. Growth Des. 15 (11) (2015) 5519–5529, https://doi.org/10.1021/acs.cgd.5b01153.
[20] F.J. Navarro-Brull, A.R. Teixeira, J. Zhang, R. Gómez, K.F. Jensen, Reduction of dispersion in ultrasonically-enhanced micropacked beds, Ind. Eng. Chem. Res. 57 (1) (2018) 122–128, https://doi.org/10.1021/acs.iecr.7b03876.
[21] L. Yang, F. Xu, Q. Zhang, Z. Liu, G. Chen, Gas-liquid hydrodynamics and mass transfer in microreactors under ultrasonic oscillation, Chem. Eng. J. 397 (2020) 125411, https://doi.org/10.1016/j.cej.2020.125411.
[22] Z. Dong, C. Yao, Y. Zhang, Hydrodynamics and mass transfer of oscillating gas-liquid flow in ultrasonic microreactors, Am. Inst. Chem. Eng. (2016) 1294–1307, https://doi.org/10.1002/aic.
[23] Q. Zhang, Z. Dong, S. Zhao, Z. Liu, G. Chen, Ultrasound-assisted gas–liquid mass transfer process in microreactors: the influence of surfactant, channel size and ultrasound frequency, Chem. Eng. J. 405 (2021) 126720, https://doi.org/10.1016/j.cej.2020.126720.
[24] C. Wang, B. Rallabandi, S. Hilgenfeldt, Frequency dependence and frequency control of microbubble streaming flows, Phys. Fluids 25 (2) (2013) 022002, https://doi.org/10.1063/1.4790803.
[25] Tandiono, S.-W. Ohl, D.S.W. Ow, E. Klaseboer, V.V. Wong, R. Dumke, C.-D. Ohl, Sonochemistry and sonoluminescence in microfluidics, Proc. Natl. Acad. Sci. 108 (15) (2011) 5996–5998, https://doi.org/10.1073/pnas.1019623108.
[26] B.E. Sarac, D.S. Stephens, J. Eisener, J.M. Rosselló, R. Mettin, Cavitation bubble dynamics and sonochemiluminescence activity inside sonicated submerged flow tubes, ArXiv 150 (2020) 1–25.
[27] F. Prabowo, C.-D. Ohl, Surface oscillation and jetting from surface attached acoustic driven bubbles, Ultrason. Sonochem. 18 (1) (2011) 431–435, https://doi.org/10.1016/j.ultsonch.2010.07.013.
[28] P. Tho, R. Manasseh, A. Ioo, Cavitation microstreaming patterns in single and multiple bubble systems, 2007. DOI:10.1017/S0022112006004393.
[29] H. Bruus, J. Dual, J. Hawkes, M. Hill, T. Laurell, J. Nilsson, S. Radel, Lab on a Chip Forthcoming Lab on a Chip tutorial series on acoustofluidics : Acoustofluidics — exploiting ultrasonic standing wave forces and acoustic streaming in microfluidic systems for cell and particle manipulation, (2011) 3579–3580. DOI:10.1039/c1lc90058g.
[30] A. Lenshof, M. Evander, T. Laurell, J. Nilsson, Acoustofluidics 5: building microfluidic acoustic resonators, Lab Chip 12 (2012) 684–695, https://doi.org/10.1039/c1lc20996e.
[31] T. Anderson, M. Anderson, O. Thomsen, Simulation of Piezoelectric Transformers with COMSOL, 2012 COMSOL Conf. (2012). http://www.comsol.com/papers/12755/.
[32] L.R. W., The theory of sound, Nature 58 (1493) (1898) 121–122, https://doi.org/10.1038/058121a0.
[33] A. Qi, L.Y. Yeo, J.R. Friend, D.P. Lagunas, Interfacial destabilization and atomization driven by surface acoustic waves, Phys. Fluids. 20 (2008) 47–60, https://doi.org/10.1063/1.2953537.
[34] R.J. Lang, Ultrasonic atomization of liquids, J. Acoust. Soc. Am. 34 (1) (1962) 6–8, https://doi.org/10.1121/1.1909020.
[35] R.W. Wood, A.L. Loomis, The physical and biological effects of high-frequency sound-waves of great intensity, J. Franklin Inst. 205 (1928) 151–153.
[36] L. Rozenberg, Physical Principles of Ultrasonic Technology, Plenum Press, New York-London, 1973.
[37] D.J. Collins, O. Manor, A. Winkler, H. Schmidt, J.R. Friend, L.Y. Yeo, Atomization off thin water films generated by high-frequency substrate wave vibrations, Phys. Rev. E - Stat. Nonlinear, Soft Matter Phys. 86 (5) (2012), https://doi.org/10.1103/PhysRevE.86.056312.
[38] M. Ashokkumar, F. Cavalieri, F. Chemat, K. Okitsu, A. Sambandam, K. Yasui, B. Zisu, Handbook of ultrasonics and sonochemistry, 2016. DOI:10.1007/978-981-287-278-4.
[39] M. Kauer, V. Belova-Magri, C. Cairós, G. Linka, R. Mettin, High-speed imaging of ultrasound driven cavitation bubbles in blind and through holes, Ultrason. Sonochem. 48 (2018) 39–50, https://doi.org/10.1016/j.ultsonch.2018.04.015.
[40] Tandiono, S.-W. Ohl, D.-W. Ow, E. Klaseboer, V.V.T. Wong, A. Camattari, C.-D. Ohl, Creation of cavitation activity in a microfluidic device through acoustically driven capillary waves, Lab Chip 10 (14) (2010) 1848, https://doi.org/10.1039/c002363a.
[41] R. Pohlman, K. Heisler, M. Cichos, Powdering aluminium and aluminium alloys by ultrasound, Ultrasonics 12 (1) (1974) 11–15, https://doi.org/10.1016/0041-624X(74)90080-8.
[42] R. Pohlman, K. Stamm, Untersuchung zum Mechanismus der Ultraschallvernebelung an Flüssigkeitsoberflächen im Hinblick auf technische Anwendungen, Westdtsch. Verlag. (1965), https://doi.org/10.1007/978-3-663-07399-4.
[43] J. Sponer, Dependence of the cavitation threshold on the ultrasonic frequency, Czechoslov. J. Phys. 40 (10) (1990) 1123–1132.
[44] K. Yasuda, H. Honma, Z. Xu, Y. Asakura, S. Koda, Ultrasonic atomization amount for different frequencies, Jpn. J. Appl. Phys. 50 (7) (2011) 07HE23, https://doi.org/10.1143/JJAP.50.07HE23.
[45] P. Sobieszuk, J. Aubin, R. Pohorecki, Hydrodynamics and mass transfer in gas-liquid flows in microreactors, Chem. Eng. Technol. 35 (8) (2012) 1346–1358, https://doi.org/10.1002/ceat.v35.810.1002/ceat.201100643.
[46] R. Mettin, Bubble structures in acoustic cavitation, A. A. Doinikov Mod. Trends Appl. Res. Signpost, Kerala. (2005) 1–36.
[47] T.G. Leighton, A.J. Walton, M.J.W. Pickworth, Primary Bjerknes forces, Eur. J. Phys. 11 (1) (1990) 47–50, https://doi.org/10.1088/0143-0807/11/1/009.
[48] R.J. Lang, Ultrasonic Atomization of Liquids, 34 (1962) 6–8. DOI:10.1121/1.1909020.
[49] K. Söllner, The mechanisms of the formation of fogs by ultrasonic waves, Trans. Faraday Soc. 32 (1936) 1532–1536.
[50] F. Barreras, H. Amaveda, A. Lozano, Transient high-frequency ultrasonic water atomization, Exp. Fluids 33 (3) (2002) 405–413, https://doi.org/10.1007/s00348-002-0456-1.

[51] K.A. Ramisetty, A.B. Pandit, P.R. Gogate, Investigations into ultrasound induced atomization, Ultrason. Sonochem. 20 (1) (2013) 254–264, https://doi.org/10.1016/j.ultsonch.2012.05.001.
[52] B. Avvaru, M.N. Patil, P.R. Gogate, A.B. Pandit, Ultrasonic atomization: effect of liquid phase properties, Ultrasonics. 44 (2) (2006) 146–158, https://doi.org/10.1016/j.ultras.2005.09.003.
[53] V. Jokanović, A.M. Spasić, D. Uskoković, Designing of nanostructured hollow TiO 2 spheres obtained by ultrasonic spray pyrolysis, J. Colloid Interface Sci. 278 (2) (2004) 342–352, https://doi.org/10.1016/j.jcis.2004.06.008.